(lifting of exact electronic degeneracies) but also by pseudo-Jahn-Teller effects (lifting of quasidegeneracies). Because exciton binding energies are generally much smaller than typical bandwidths, it would be a most remarkable accident if even in one crystal the excitonic instability were actually to generate a phase transition.

It is known that in grey Sn contact between valence and conduction bands actually occurs. Here, for sandwich structures long before crossing or contact occurs, the structure becomes unstable. We attribute this instability to the cooperation of the "small-gap" mechanism (which simply decreases the energy gained from forming bonds) with the M^+—M^+ repulsion discussed in Sec. III. The cooperation of these two mechanisms makes the sandwich structure (based on an odd number of electrons per atom pair) inherently less stable than A^NB^{8-N} structures, which are stabilized in the same manner as alternating hydrocarbons.[16]

The fact observed here that the In—In bond length is abnormally large implies that the In—In bonds are unusually weak. In GaSe fine structure associated with the emission of four phonons has been observed.[15] In InSe it is expected that this fine structure should be much richer, so that investigation of the spectrum of InSe near 1.1 eV at low temperatures appears warranted.

The discussion given here is intended to encompass materials with covalent structures associated with hybridized s-p bonds. It does not apply to transition or rare-earth metal salts, where an intra-atomic mechanism (transfer of charge from localized and possibly magnetic d or f states to delocalized s-p states) may give rise to an insulator-metal transition. In all cases, however, it appears that structural changes are associated with the properties of *all* the valence electrons, not merely those confined to small regions of momentum space near band edges.

PHYSICAL REVIEW VOLUME 188, NUMBER 3 15 DECEMBER 1969

Excitonic Molecule Bound to the Isoelectronic Nitrogen Trap in GaP

J. L. Merz, R. A. Faulkner, and P. J. Dean
Bell Telephone Laboratories, Murray Hill, New Jersey 07974
(Received 22 July 1969)

Two sets of sharp emission lines, associated with the photoluminescence spectrum of the isoelectronic nitrogen trap in GaP, are unambiguously identified as the recombination of a second exciton bound to this center with an energy of 10 meV. This is the first observation of an excitonic molecule bound at a defect. The two electrons and two holes within this complex combine to form two antisymmetric states of angular momentum $J_t=0$ and $J_t=2$. The $J_t=2$ state is split 0.16 meV by the cubic crystal field, and the $J_t=0$ state lies 0.17 meV above the center of gravity of this doublet. Transitions from these states to the A and B states of a single exciton bound to nitrogen are seen. The complex Zeeman splittings predicted by this model agree in detail with experiment. The excitonic molecule is stable at low temperature; at 1.5°K, the excitonic molecule emission lines increase as the square of the single exciton intensity with increase in pumping power. However, nonradiative Auger recombination reduces the over-all nitrogen emission by a factor of 3 below the intensity at 4.2°K. The binding energy of the second exciton at the nitrogen trap is nearly equal to that of the single exciton. This remarkable fact may be possible only for an isoelectronic trap.

I. INTRODUCTION

THE optical spectra produced when nitrogen is substituted isoelectronically for phosphorus in GaP have been investigated in detail, both by experiment and theory.[1–9] For dilute concentrations of nitrogen ($\lesssim 10^{17}$/cc), a pair of no-phonon lines plus their optical and acoustic phonon replicas are observed from the recombination of an exciton bound to the isolated nitrogen impurities. These no-phonon lines result from the coupling of a spin $S=\frac{1}{2}$ electron from the conduction band and a $J=\frac{3}{2}$ hole from the topmost valence band to produce two bound states of total angular momentum $J_t=1$ and 2, located approximately 11 meV below the free exciton level, and separated by 0.87 meV. Spectral lines originating from transitions between these states and the $J_t=0$ ground state have been designated the A and B lines, respectively.[3,4] The

[1] D. G. Thomas, M. Gershenzon, and J. J. Hopfield, Phys. Rev. **131**, 2397 (1963).
[2] Y. Yafet and D. G. Thomas, Phys. Rev. **131**, 2405 (1963).
[3] D. G. Thomas, J. J. Hopfield, and C. J. Frosch, Phys. Rev. Letters **15**, 857 (1965).
[4] D. G. Thomas and J. J. Hopfield, Phys. Rev. **150**, 680 (1966).
[5] J. J. Hopfield, D. G. Thomas, and R. T. Lynch, Phys. Rev. Letters **17**, 312 (1966).
[6] J. D. Cuthbert and D. G. Thomas, Phys. Rev. **154**, 763 (1967).
[7] J. J. Hopfield, P. J. Dean, and D. G. Thomas, Phys. Rev. **158**, 748 (1967).
[8] R. A. Faulkner and J. J. Hopfield, in *Proceedings of the International Conference on Localized Excitations in Solids*, edited by R. F. Wallis (Plenum Press, Inc., New York, 1968), p. 218.
[9] Roger A. Faulkner, Phys. Rev. **175**, 991 (1968).

higher-energy A-line transition ($\Delta J_t=1$) is dipole-allowed, whereas the B line ($\Delta J_t=2$) is forbidden and can be observed in photoluminescence only at low temperatures ($T\leq\sim 5°K$) because of thermalization. Strain or an external magnetic field mixes the $J_t=1$ and 2 states, increasing the relative strength of the B line.[10]

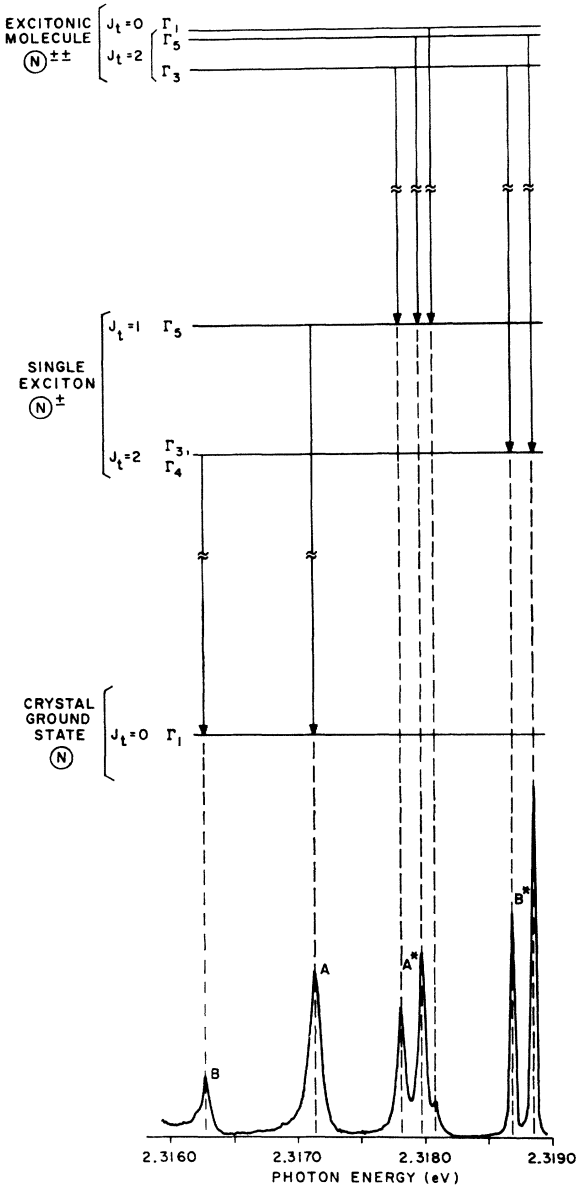

FIG. 1. Photoluminescence spectrum and energy-level diagram of the isoelectronic nitrogen trap in GaP. Lines A and B arise from the decay of the $J_t=1$ and $J_t=2$ states of a single exciton bound to nitrogen. Lines A^* and B^* result from the radiative decay of the $J_t=0$ and $J_t=2$ (crystal-field split) states of the excitonic molecule bound to nitrogen, the final states of the transitions being the $J_t=1$ (A line) and $J_t=2$ (B line) states, respectively, of the single exciton. Symmetries of the energy levels are given in the notation of Koster *et al.* (Ref. 14).

[10] This has been demonstrated quantitatively for an applied magnetic field in the analogous case of the isoelectronic oxygen trap in ZnTe. See J. L. Merz, Phys. Rev. 176, 961 (1968).

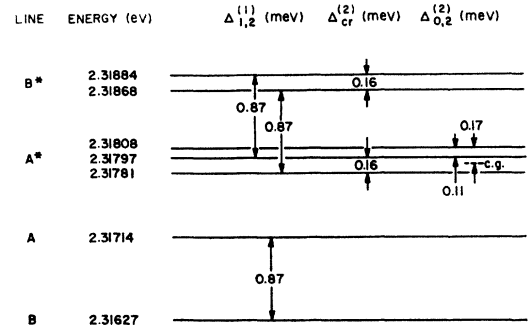

FIG. 2. Energies of the excitonic molecule (A^*-B^*) lines and the single-exciton (A-B) lines. Absolute energies are correct to ± 0.02 meV, relative energies to less than ± 0.01 meV. The energy-level diagram for the spectral lines shown here is given in Fig. 1. Important spacings of the spectral lines are indicated by arrows. $\Delta_{1,2}^{(1)}$ is the separation of the $J_t=1$ and 2 states of the single exciton. $\Delta_{cr}^{(2)}$ is the crystal-field splitting of the $J_t=2$ state of the excitonic molecule. $\Delta_{0,2}^{(2)}$ is the separation of the $J_t=0$ and 2 states of the excitonic molecule.

It has thus been demonstrated that isoelectronic nitrogen can bind an exciton in GaP. The present work reports an experimental and theoretical study of a new effect: the binding of a pair of excitons to a nitrogen atom.[11] The free excitonic molecule (two excitons bound together to form a mobile four-particle system) has been observed by Haynes[12] in Si and later in other materials; however, this is the first observation of an excitonic molecule bound to a defect.

The luminescence spectrum investigated in this work consists of two sets of sharp lines which are observed at energies slightly higher than the A and B lines. These lines are observed in photoluminescence but not in absorption. A high-resolution spectrum showing these two sets of lines[13] (designated A^* and B^*) along with the A-B lines is shown in Fig. 1. Under favorable excitation conditions (to be discussed in Sec. V), the A^*-B^* lines can be made strong relative to A-B, as shown. The energies of the seven lines in this spectrum are listed in Fig. 2, and the relevant energy spacings of these lines are emphasized.

Previous misguided speculation about the origin of these lines prompted the suggestion that they were higher valley-orbit states of the electron in the single exciton bound to nitrogen.[9] However, the detailed investigation of the behavior of these lines reported in this paper shows that they result from the radiative recombination of one of the two excitons comprising the bound excitonic molecule, leaving a single exciton

[11] A preliminary account of this work has been given in R. A. Faulkner, J. L. Merz, and P. J. Dean, Solid State Commun. 7, 831 (1969). Some of the results contained therein (e.g. calculated values of the electron and hole g factors) have been corrected slightly in the present paper after additional calculations based on more accurate data.

[12] J. R. Haynes, Phys. Rev. Letters 17, 860 (1966).

[13] The nomenclature for A^* and B^* has been reversed in the present paper (and in Ref. 11) compared with the arbitrary assignment in Ref. 9, because these lines result from transitions to the A and B states, respectively.

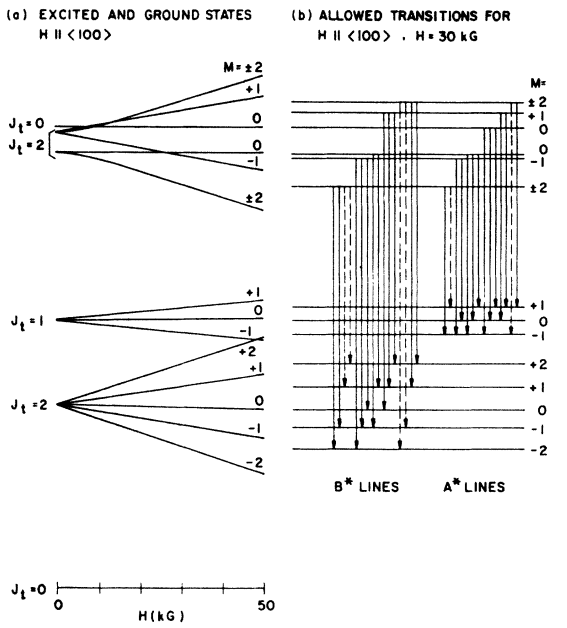

FIG. 3. (a) Magnetic-field splittings of the excitonic molecule and single-exciton states for the field in a ⟨100⟩ crystallographic direction. The excitonic molecule levels labeled ±2 are equal linear combinations of the $M=+2$ and -2 magnetic states at low field and become pure $M=+2$ and -2 at high fields. (b) Dipole-allowed transitions for the states at $H=30$ kG. Solid arrows indicate dipole transitions allowed for all values of field; broken arrows are transitions allowed only at low fields ($H<25$ kG).

bound to nitrogen in the ground state. The A^* and B^* lines are radiative transitions which originate from the excitonic molecule states and terminate on the $J=1$ (A-line) and $J=2$ (B-line) states, respectively, of the single exciton, as shown in Fig. 1. The intensity of the A^*-B^* lines increases as the square of the A-B lines with increasing excitation intensity, as expected for this model.

II. THEORY

The excitonic molecule (or double exciton) in GaP consists of two electrons with spin $S=\frac{1}{2}$ in valley-orbit singlet states and two holes with angular momentum $J=\frac{3}{2}$. The electrons can only couple with anti-parallel spins and contribute no net angular momentum. Simple vector coupling of the $J=\frac{3}{2}$ angular momenta of the holes results in states with total angular momentum $J_t=3$, 2, 1, and 0. Of these, the Pauli principle excludes all but the anti-symmetric states $J_t=2$ and 0. The cubic crystal field of the GaP lattice (T_d symmetry) can split the $J_t=2$ state into a twofold degenerate state with symmetry Γ_3 and a state of threefold degeneracy with symmetry Γ_5.[14] We observe this crystal-field splitting to be 0.16 meV (cf. Fig. 2). The $J_t=0$ state has Γ_1 symmetry and is located 0.11 meV above the higher Γ_5 state (or 0.17 meV above the center of gravity of the $J_t=2$ states). These states are shown in Fig. 1, and the allowed transitions to the A and B lines are indicated.

The ground states of the transitions are the $J_t=1$ and 2 levels of the single exciton. The $J_t=1$ state has Γ_5 symmetry, and the $J_t=2$ state can split into Γ_3 and Γ_4 levels. The crystal-field splitting is unobservably small for the $J_t=2$ state of the single exciton. Transitions from the $J_t=0$ and 2 excited states are dipole-allowed to the $J_t=1$ ground state (A line of the single exciton), producing three A^* lines with separations derived from the excited states. However, for transitions terminating on the $J_t=2$ ground state (B line of the single exciton), only transitions from the $J_t=2$ excited state are allowed, since transitions from the $J_t=0$ excited state involve $\Delta J_t=2$ and are forbidden. Therefore, only two B^* lines are seen, whose separation is identical to that of the two lower-energy lines in the A^* set. These lines lie above the corresponding A^* lines by exactly the separation between the A and B lines (Fig. 2).

To calculate the splittings of these states in an applied magnetic field, the magnetic interaction matrices have been diagonalized for the Γ_1, Γ_3, and Γ_5 excited states and the Γ_3, Γ_4, and Γ_5 ground states. Group theory shows that only two independent constants are needed to describe the magnetic behavior of the excited states, while five constants are required for the ground states. The details of these calculations are given in the Appendix. For the magnetic field in a ⟨100⟩ crystallographic direction, the energy eigenvalues can be calculated analytically. For other directions the energy levels have been obtained numerically.

The results for these calculations in the [100] direction are shown in Fig. 3. Dipole-allowed transitions are indicated by arrows, using the selection rules $\Delta J_t=0$, ±1 and $\Delta M=0$, ±1 (except $J_t=2$, $M=0$ to $J_t=2$, $M=0$, which is dipole-forbidden). For low values of magnetic field, 16 transitions are allowed to the $J_t=2$ ground state, while only 12 are allowed at high fields, where the highest and lowest states of the excitonic molecule are pure $M=+2$ and -2 states, respectively. There are 14 allowed transitions to the $J_t=1$ ground state at low field, and 12 at high field. The values of the magnetic interaction constants have been determined by fitting the experimental data for the sharpest lines observed in the [100] orientation, as discussed in Sec. IV.

To give these interaction constants physical significance, they can be related to electron and hole g factors of an effective spin Hamiltonian. This is done in the Appendix.

III. EXPERIMENTAL

A. Crystal Growth

Small strain-free platelet crystals of GaP were grown from gallium solution at ~1100°C. An open-tube fur-

[14] Group-theoretical notation and conventions used here are those of Koster *et al.*, *Properties of the Thirty-Two Point Groups* (M.I.T. Press, Cambridge, Mass., 1963).

nace system designed to provide minimal impurity concentrations[15] was used. Crystals grown both with Al_2O_3 and with SiO_2 furnace tubes and boats were suitable, containing $\lesssim 10^{15}$ nitrogen cm^{-3} and sulphur and carbon concentrations sufficiently low that donor-acceptor pair luminescence spectra were not seen. Some crystals were prepared using phosphine generated from AlP as the source of phosphorus; others were grown using red phosphorus.

B. Photoluminescent Spectra

Photoluminescence was excited with 4880 Å radiation from an argon-ion laser, focused onto the sample immersed in liquid helium. The intensity of the laser radiation was measured with a calibrated Eppley thermopile. Measurements were taken at 4.2 and 1.5°K. For magnetic fields up to 30.5 kG, a Varian electromagnet was used and the spectra were recorded photographically on a 2-m Bausch and Lomb spectrograph using a 1200-groove/mm grating in third order. Absolute energies of spectral lines could be determined to ±0.02 meV and relative energies of lines in a given spectrum to ±0.005 meV. The magnetic subcomponents were sufficiently sharp to enable splittings as small as 0.01 meV to be resolved in the best crystals. Most studies of the orientational dependence of the magnetic field were carried out with this apparatus, since the crystal could be rotated about a ⟨110⟩ axis perpendicular to the field. Magnetic fields of up to 50 kG were obtained using a Westinghouse superconducting solenoid. A 1-m Jarrell-Ash Czerney-Turner spectrometer, with a 1180-groove/mm grating blazed at 1.1 μ, was used in third order in conjunction with the superconducting magnet. This magnet had room-temperature access to the solenoid bore, so the samples, mounted in a separate helium cryostat, could be pumped below the λ point independent of the magnet cryogenics. Accurate sample orientation was more difficult to achieve in this magnet and the energy resolution with this apparatus was degraded by nearly a factor of 2 over the figures given above.

With the use of focused laser radiation, small areas of the crystals (<0.1 mm diam) could be excited to find strain-free regions. The presence of internal crystal strain could be sensitively detected by monitoring the strain-induced splitting of the *C* line, which results

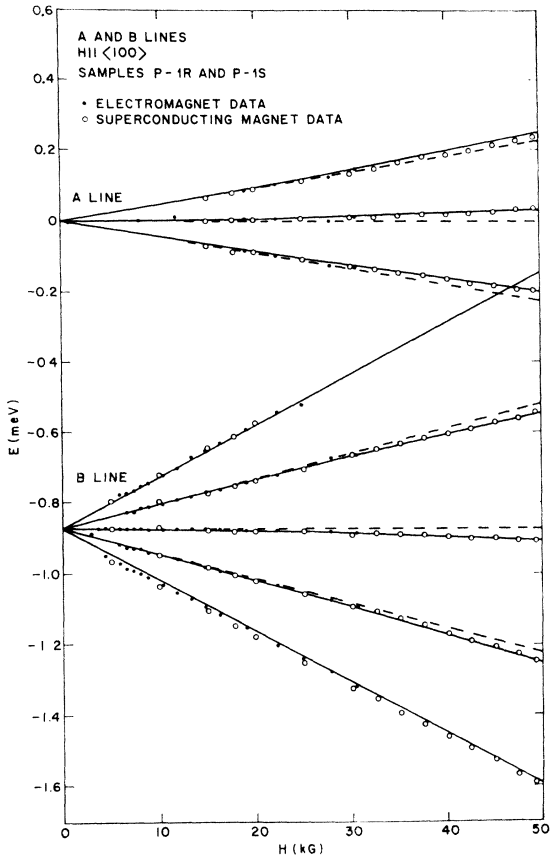

FIG. 4. Zeeman splittings of the *A* and *B* single-exciton lines, for **H**‖⟨100⟩. Energies are measured relative to the zero-field *A* line at 2.31714 eV. Solid curves are the theory, solid and open circles are data points. Size of circle indicates experimental accuracy. The deviation of the $M=0$, ±1 components from linearity (dashed lines) results from the interaction between *A* and *B* at high fields. At low fields ($H<15$ kG) the three components of the *A* line could not be resolved. At high fields ($H>25$ kG) the $M=+2$ component of the *B* line could not be seen because of thermalization. Five theoretical parameters have been determined from this single-exciton data.

[15] P. J. Dean, C. J. Frosch, and C. H. Henry, J. Appl. Phys. 39, 5631 (1968).

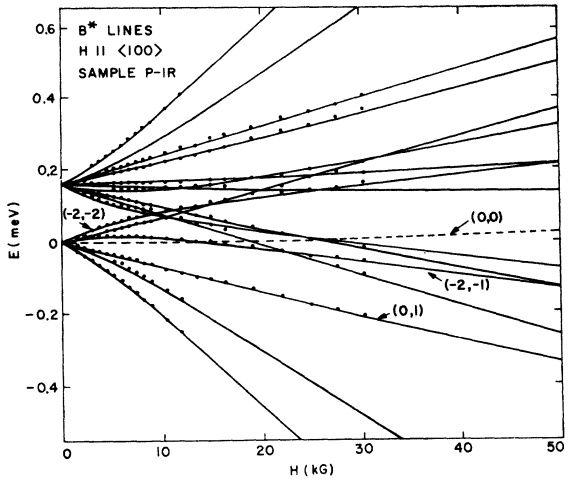

FIG. 5. Zeeman splittings of the B^* lines of the excitonic molecule, for **H**‖⟨100⟩. Solid and dashed curves are theory, circles are data. Energies are measured relative to the lower zero-field B^* line at 2.31868 eV. The dashed curve (0,0 transition) is dipole-forbidden. The other transitions labelled (i,f) are predicted and observed to be strong (cf. text). The initial and final states for the transitions shown here are given in Fig. 3. Only two additional parameters (plus the zero-field splitting) were needed to fit theory to experiment. These two parameters were determined solely from the data shown in this figure and were used without alteration for all further calculations.

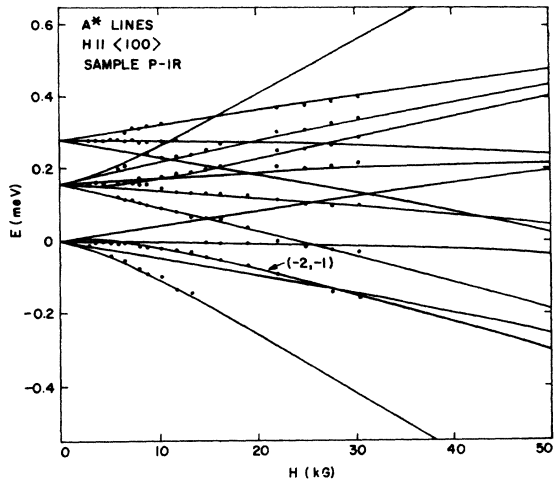

FIG. 6. Zeeman splittings of the A^* lines, for $\mathbf{H}\|\langle 100\rangle$. Solid curves are theory; circles are data. Energies are measured relative to the lowest zero-field A^* line at 2.31781 eV. The $(-2, -1)$ transition is predicted and observed to be strong. The initial and final states for the transitions shown here are given in Fig. 3. These results provide an independent check of the theory.

from the radiative recombination of excitons bound to neutral sulfur donors inadvertently present in the crystals.[16]

Relative intensities of spectral lines were measured photoelectrically with an EMI 9558Q photomultiplier and the 1-m Jarrell-Ash spectrometer.

IV. MAGNETIC-FIELD EFFECTS

The magnetic-field splitting of the A and B lines of the single exciton and the B^* lines of the excitonic molecule are shown in Figs. 4 and 5, for $\mathbf{H}\|\langle 100\rangle$. The deviation from linearity of the $M=0, \pm 1$ components of the A and B lines at large magnetic field results from the repulsive interaction between the A and B lines; this effect determines two of the five interaction constants. All five of the single exciton interaction constants have been determined by fitting the A- and B-line of data of Fig. 4. Using these constants determined solely from the properties of the single exciton, only two additional interaction constants were needed to fit the B^* data of the excitonic molecule, shown in Fig. 5. One other constant, the crystal-field splitting of the $J_t=2$ excited state, was taken from the zero-field data. The values of the interaction constants obtained in this way are listed in Table I, and these values have been used for numerical calculations of magnetic splittings for all the other figures discussed below.

In addition to the close fit of theory and experiment for the magnetic splittings of these lines, the observed intensities are in reasonable agreement with the transition probabilities calculated from the states involved, when thermalization effects are taken into account. For example, the lines labelled $(-2, -2)$, $(-2, -1)$, and (0,1) in Fig. 5 result from the following transitions: (i,f) is a transition from the excitonic molecule state $|J_t=2, M=i\rangle$ to the single exciton state $|J_t=2, M=f\rangle$. The transition probability for (0,1) is relatively large and the observed line is medium to strong in intensity. Lines $(-2, -2)$ and $(-2, -1)$ are expected to be strong because of thermalization in the excited state, and these lines are observed to be strong. Transition (0,0) is dipole-forbidden and is not observed.

One independent check of the theory is provided by the A^* lines of the excitonic molecule, shown in Fig. 6. These lines are not as sharp as the B^* lines, because the ground state (A line) is broad. However, additional information is contained in the A^* data, since transitions from the $J_t=0$ state of the excitonic molecule are allowed; transitions from this state are seen to be identical with the A-line splitting, as anticipated. The line labelled $(-2, -1)$ in Fig. 6 is observed to be the strongest line in the spectrum. This is the

TABLE I. Measured and derived Zeeman constants for the single and double excitons bound to N in GaP. Measured quantities are defined in Tables II and III. Derived quantities are defined through Appendix equations (A3), (A4), and (A8) and relate to the spin Hamiltonians (A2) and (A7). Comparison is made with earlier g value measurements of Yafet and Thomas.

	This work	
Measured quantities	Derived quantities[a]	Yafet and Thomas[b]
$\gamma_1=0.77\pm0.01$	$K_1=0.95\pm0.04$	$K_1=0.77\pm0.16$
$\gamma_2=1.23\pm0.01$	$L_1=0.03\pm0.02$	$L_1=0.11\pm0.07$
$\gamma_3=1.25\pm0.01$	$g_e=1.96\pm0.03$	$g_e=2.02\pm0.12$
$\delta_1=-0.31\pm0.01$	$\frac{1}{2}(\gamma_1-\gamma_2)=-0.23\pm0.01$	
$\delta_2=-0.31\pm0.01$	$\frac{1}{2}(\gamma_1+\gamma_2)-\gamma_3=-0.25\pm0.02$	
$\zeta_1=1.08\pm0.01$	$K_2=0.89\pm0.03$	
$\zeta_2=0.99\pm0.01$	$L_2=0.06\pm0.01$	

[a] Minor corrections have been made to these values since the preliminary account of this work, Ref. 11.
[b] Reference 2.

[16] P. J. Dean, Phys. Rev. 157, 655 (1967).

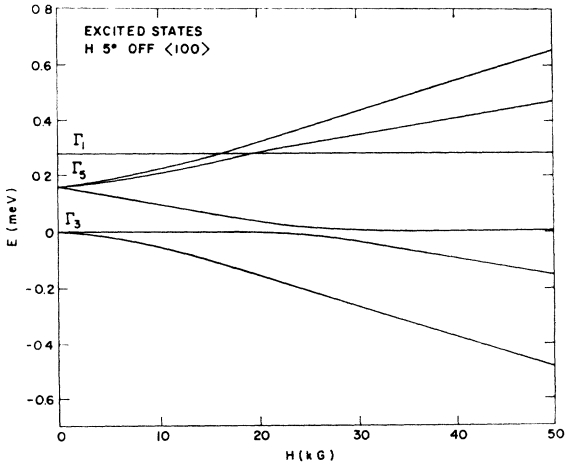

FIG. 7. Calculated splittings of the excitonic molecule states for the magnetic field at an angle of 5° from a $\langle 100\rangle$ direction. Note that levels which crossed for $\mathbf{H}\|\langle 100\rangle$ (Fig. 3) are repelled in this orientation.

$|2,-2\rangle \rightarrow |1,-1\rangle$ transition, and is again expected to be strong because of thermalization.

Figures 7 and 8 show the Zeeman splitting of the excitonic molecule up to 50 kG; the data were taken in a superconducting magnet where crystal alignment was less precise and spectral resolution poorer than the data in Figs. 5 and 6. The best fit of theory and experiment was obtained for the magnetic field at an angle of 5° from a ⟨100⟩ crystal axis. (The deviation from ⟨100⟩ is effectively isotropic for angles of deviation less than 20°.) Figure 7 shows the calculated energy levels of the excitonic molecule states for this orientation: The ground states (single exciton states) are nearly isotropic as a function of field direction, as will be demonstrated below. Figure 8 gives the calculated and observed transitions for A^* and B^* from the excited states shown in Fig. 7 to the A and B lines, respectively.

It should be noted that levels which crossed in a ⟨100⟩ direction (cf. Fig. 3) are repelled when the field deviates from this direction, and that the (0,0) transition, forbidden in a ⟨100⟩ direction, is now partially allowed due to mixing with other states. This orientation, therefore, gives additional information and provides further confirmation of the correct choice of parameters determined from Figs. 4 and 5.

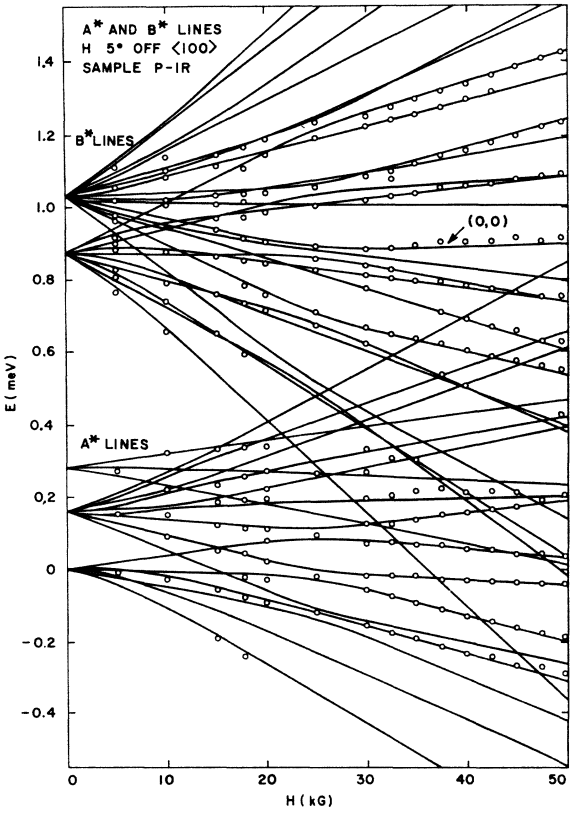

FIG. 8. High-field Zeeman splittings of the A^* and B^* lines, for the field at an angle of 5° from the ⟨100⟩ direction. The (0,0) transition is partially allowed for this orientation.

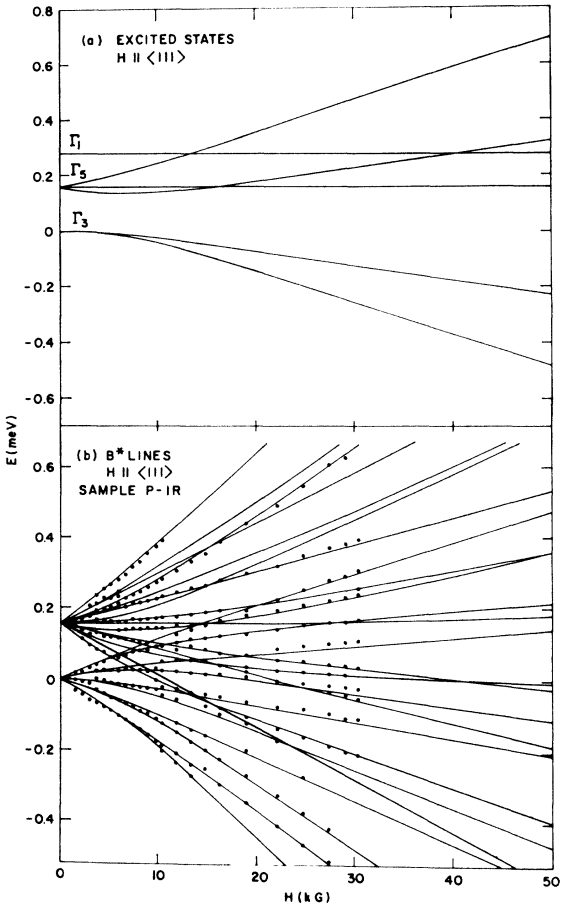

FIG. 9. Zeeman splittings of the B^* lines, for $\mathbf{H}\|\langle 111\rangle$. (a) Excitonic molecule states; (b) observed and calculated transitions. Note that more transitions are allowed than for $\mathbf{H}\|\langle 100\rangle$.

The measured B^* transitions for $H\|\langle 111\rangle$ and $H\|\langle 110\rangle$ are compared with theory in Figs. 9 and 10. In Figs. 11 and 12, the dependence of the B^* lines on the orientation of the field is shown as H is rotated in the $\langle 1\bar{1}0\rangle$ plane from the ⟨110⟩ to the ⟨001⟩ directions, for a constant magnetic field of 30.5 kG. The splitting of the excited and ground states giving rise to the B^* transitions are shown in Fig. 11. Both the $J_t=2$ (B line) states of the single exciton (ground states shown in Fig. 11) and the $J_t=1$ states (A line; not shown in Fig. 11) are found to be closely isotropic.[17] Therefore, most of the anisotropy of the B^* lines is due to the excited states. The magnetic quantum numbers M shown in Fig. 11 are for $\mathbf{H}\|\langle 001\rangle$; for other orientations M is not a good quantum number because of mixing of the states. The central component of the ground state is displaced 0.015 meV below the energy zero because of the nonlinear shifts of the A and B lines (cf. Fig. 4). The B^* transitions among these states are

[17] The splittings of the A and B lines were also found to be effectively isotropic in the lower spectral resolution study made by Yafet and Thomas (Ref. 2).

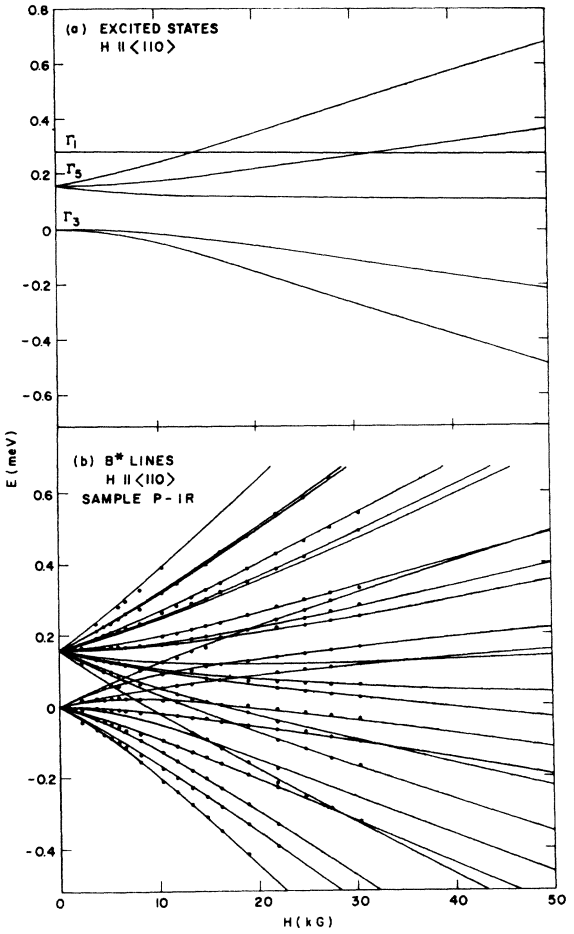

FIG. 10. Zeeman splittings of the B^* lines, for $\mathbf{H}\|\langle 110\rangle$. (a) Excitonic molecule states; (b) observed and calculated transitions.

shown in Fig. 12. All transitions are labelled for $\mathbf{H}\|\langle 001\rangle$, where the magnetic quantum numbers are valid. As before, (i,f) refers to the transition

$$|J_t=2,\ M=i\rangle \rightarrow |J_t=2,\ M=f\rangle.$$

All transitions involving $\Delta M=2$ and $M=0\rightarrow 0$ are dipole-forbidden and are not observed for $\mathbf{H}\|\langle 001\rangle$. For other orientations, some of these transitions become allowed; thus, transitions (0,0) and $(-1, 1)$ are observed at $\theta=35°$ and 45°. (This effect was also noted in Fig. 8.)

From the results presented above, g factors have been calculated for the appropriate Zeeman Hamiltonians given in the Appendix. These are listed in Table I. The values obtained by Yafet and Thomas for the single exciton[2] are given for comparison. Lower error limits are given for the values obtained in this work, because of the higher spectral resolution used. The two sets of values are seen to agree to within experimental error. In addition, the hole g factors are very nearly equal for the single and double excitons.

V. DEPENDENCE ON INTENSITY OF EXCITATION

The model of the excitonic molecule proposed here to explain the A^* and B^* lines in the nitrogen spectrum predicts that these lines should increase as the square of the intensity of the single exciton lines. This dependence has been investigated. Figure 13 shows a log-log plot of the intensity of the high-energy line of the B^* doublet, and the intensity of the A line, as a function of the intensity of the laser excitation source. At low excitation intensity (≤ 0.1 mW) the growth of the A line is linear with a slope of 0.9. In this same region the B^* line increases linearly with a slope of 1.8, exactly twice that of the A line, as expected. The deviation of these slopes from the expected values of 1.0 and 2.0 is outside the limits of experimental error and is not understood, but the square-law dependence of the luminescence intensity of the excitonic molecule

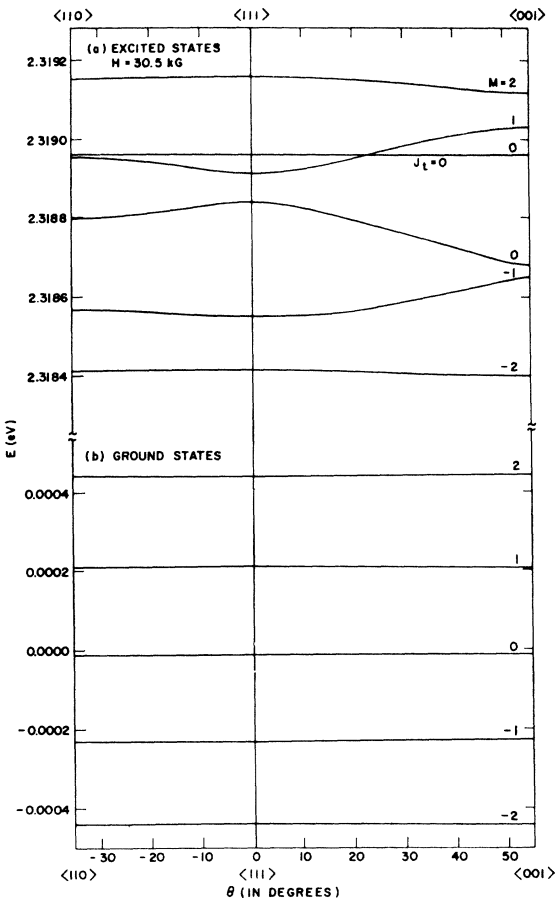

FIG. 11. Orientational dependence of the excited states (a) and the ground states (b) of the B^* transitions at 30.5 kG. Energy is plotted in eV's relative to the zero-field B line. θ is the angle between a ⟨111⟩ crystallographic direction and the magnetic field, as the crystal is rotated in the $(1\bar{1}0)$ plane. Major crystallographic directions are indicated. The $J_t=0$ state of the excitonic molecule is indicated; all other excited and ground states have $J_t=2$. Magnetic quantum numbers M listed are for $\mathbf{H}\|\langle 001\rangle$, the only orientation for which these quantum numbers are strictly valid. Ground states are very nearly isotropic.

(B^*) on that of the single exciton (A) has been demonstrated. At higher excitation intensity (from $\sim$0.2 to $\sim$10 mW), the A line begins to saturate, and the B^* line grows with a slope approaching unity, again as expected. Above approximately 10-mW excitation power, the crystal begins to heat above the temperature of the bath, 1.5°K. This heating can be observed by monitoring the ratio of the B line to the A line, also shown in Fig. 13. When the crystal begins to heat, the B/A ratio is reduced because of thermalization. Heating causes the A line to grow rapidly, with a corresponding decrease in the radiative lifetime of the single-exciton transition. (The lifetimes of the dipole-allowed A line and the forbidden B line differ by two orders of magnitude.[6]) This temperature-induced decrease in the lifetime of the single exciton causes the double-exciton intensity (B^* line) to decrease relative to the A line.

Figure 13 also demonstrates the experimental conditions under which the excitonic molecule lines are most easily observable. For excitation intensities between approximately 8 and 20 mW, the B^* line is stronger than the A line. The spectrum shown in Fig. 1 was taken for a pumping power of approximately 10 mW, with the bath at 1.5°K.

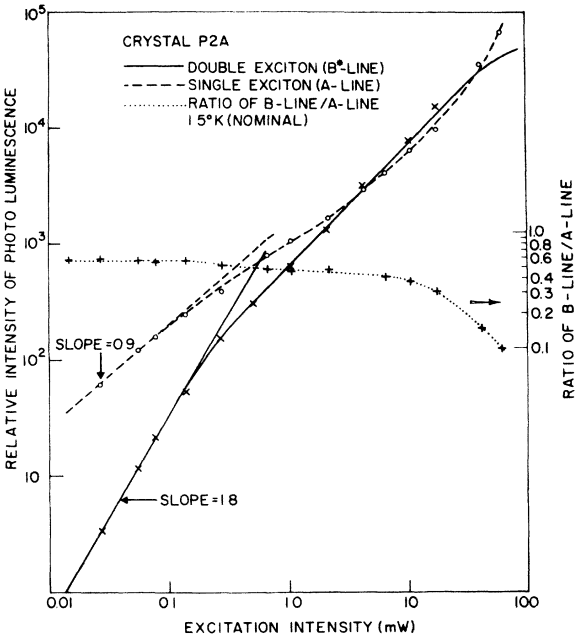

FIG. 13. Dependence of the intensity of the A line and high-energy B^* line on excitation intensity. At low excitation intensity the excitonic molecule (B^*) grows as the square of the single exciton (A). At high excitation intensity, crystal heating occurs, as shown by the decrease of the B/A ratio.

VI. MULTIPLE-PARTICLE TRANSITIONS

A. Auger Effect

The presence of four particles in the bound excitonic molecule suggests that nonradiative Auger recombinations may occur which are not possible for the single exciton. One of the two excitons in the molecule can recombine, giving its entire energy to excite the remaining exciton into the conduction band. This effect has been observed for the recombination of an exciton bound to neutral donors in GaP and Si,[18] where the exciton decay excites the donor electron. In this latter case, the Auger effect drastically reduces the radiative efficiency of excitons bound to neutral donors. The luminescence efficiency is reduced by a factor of approximately 500 for GaP and 5000 for Si.

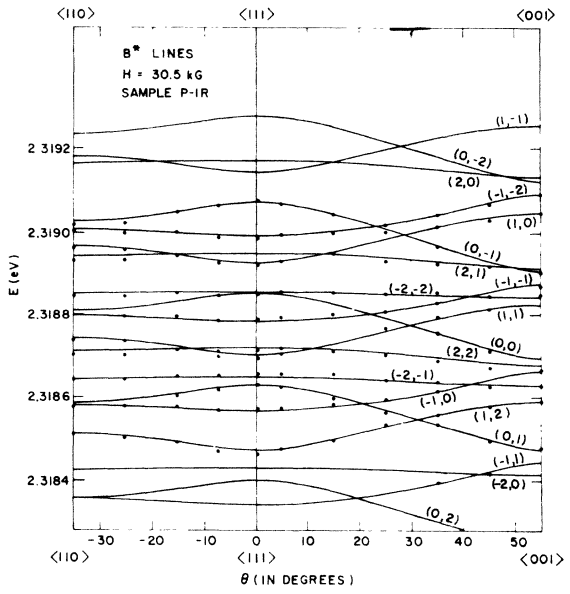

FIG. 12. Orientational dependence of the B^* lines at 30.5 kG. Solid lines are theoretical transitions calculated from the excited and ground states shown in Fig. 11. Solid circles are data points. All transitions are identified by the magnetic quantum numbers of the initial and final states (i,f) appropriate for $\mathbf{H}\|\langle 001\rangle$. Agreement is obtained between theory and experiment for allowed and forbidden transitions (cf. text).

The effect of Auger transitions on the bound excitonic molecule has been investigated by comparing spectral intensities at 4.2 and 1.5°K. At 4.2°K, the A line is strong relative to B, A^*, and B^* because of the temperature-dependent lifetime of the single exciton transition, as discussed in Sec. V. As the temperature is decreased to 1.5°K, the intensities of the A^* and B^* lines grow very rapidly relative to A, as expected, but the over-all intensity of the nitrogen luminescence ($A+B+A^*+B^*+$phonon replicas) decreases by a factor of 3. This decrease is attributed to the Auger effect. There is a redistribution of energy among the phonons during this temperature change, since the integrated intensity of the no-phonon lines alone (excluding phonon replicas) decreases by a factor of 10 in the same temperature range. This Auger effect has been observed with the same reduction in intensity in all samples examined.

[18] D. F. Nelson, J. D. Cuthbert, P. J. Dean, and D. G. Thomas, Phys. Rev. Letters 17, 1262 (1966).

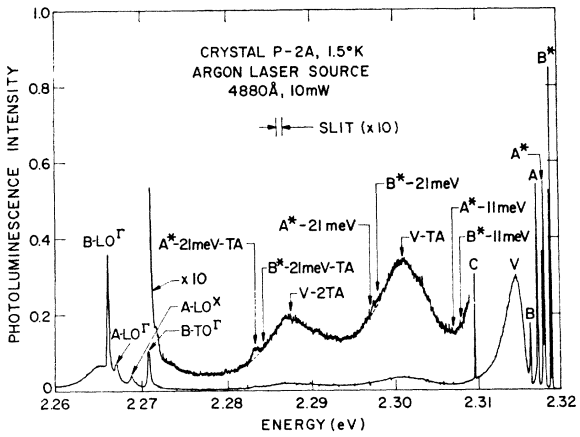

FIG. 14. Photoluminescence spectrum of GaP:N showing no-phonon lines and phonon replicas. The arrows indicate where multiple-particle recombination processes might be observed (cf. text: Sec. VI B). The origin of the V band is described in the text. LO, TO, and TA refer to various longitudinal and transverse optical and acoustic phonons which have been measured by Dean in GaP (Ref. 16). The C line results from the radiative recombination of an exciton bound to a neutral sulfur donor (Ref. 16).

The threefold reduction in luminescence intensity resulting from the Auger effect can be quantitatively accounted for by lifetime measurements. The radiative lifetime of the A line has been determined by Cuthbert and Thomas[6] to be $\sim$40 nsec. The double-exciton lines were also studied by Cuthbert and Thomas (although their origin was not properly understood at that time) and a radiative lifetime of $\sim$10 nsec was found for the A^*-B^* lines.[6] Recent unreported measurements of these lines[19] confirm the initial lifetime to be 7.5 ± 1 nsec, although their decay is found to be nonexponential, a fact which is not understood at this time. Thus, lifetime measurements predict an Auger-induced decrease of a factor of 5 or 6, in reasonable agreement with the factor of 3 observed, especially in view of the fact that single-exciton decay which is unaffected by the Auger process makes some contribution to the measured luminescence intensities (incomplete saturation). It should be noted that the Auger effect is not so disastrous for the efficiency of the double-exciton transitions as for excitons bound to neutral donors, because the radiative lifetime is much shorter ($\sim$40 nsec; cf. $\sim$11 μsec), but the lifetime for the Auger process does not change very much between these two exciton complexes. The slight increase in the Auger rate for the bound excitonic molecule compared with the donor-exciton complex ($\sim$7-nsec lifetime; cf. $\sim$21 nsec) may be attributable to the fact that the transition energy may be carried off by either a free hole or a free electron (or both) in the former case, whereas only a free electron can be ejected from the donor-exciton complex.

[19] J. D. Cuthbert (private communication).

B. Other Multiple-Particle Transitions

For the free-excitonic molecule in Si, Haynes[12] observed a transition where one of the excitons recombined, exciting the remaining exciton into the high density-of-states region at the bottom of the conduction band. In addition to this process (called process 1) for the bound excitonic molecule, a second process (process 2) is possible: One exciton may recombine and excite the second exciton into the free-exciton level in GaP. Processes 1 and 2 should produce bands 21 and 11 meV, respectively, below the energy of the A^*-B^* lines.

Figure 14 is a photoelectric recording of the no-phonon single and double-exciton lines and their phonon replicas. The band peaking at 2.315 eV (labelled V in Fig. 14) is believed to arise from the B line in the following way. An exciton in the $J_t=2$ state (B line) makes a virtual transition to the $J_t=1$ state (A line), emitting a phonon of energy approximately equal to the A-B separation. This process has been investigated in oxygen-doped ZnTe[5,20] (an analogous isoelectronic trap), where phonons of energy equal to the relatively large A-B splitting are involved (i.e., the V-band peak and the A and B lines are equally spaced). For GaP, however, the phonon density of states curve is known to be zero at low phonon energies,[21] and this density-of-states curve must be folded into the calculation of the resonant transition. This would cause the V band to peak at energies lower than the A-B separation, as observed. Two transverse acoustic phonon replicas of the V band are also seen in Fig. 14. Transverse acoustic phonon replicas of the B line cannot be seen against these strong V replicas.

The arrows in Fig. 14 indicate the expected energies for the multiple-particle processes 1 and 2. No evidence is found for process 2. A weak band is observed on the low-energy side of the V-band phonon replicas, at the energy expected for process 1. This band is reproducible for the crystal shown, and others from the same growth run, but not in other crystals examined to date. However, all the other samples examined have properties which are adverse for the detection of these weak bands. To observe process 1, the A^* and B^* lines must be strong relative to A, B, and the V band, as is the case shown in Fig. 14. Other crystals examined usually have stronger B lines and V bands, for reasons which are not fully understood. (Internal crystal strain may be present, which increases the strength of B.) In some crystals additional, unidentified lines are present in the region of the acoustic phonon replicas which also obscure the weak bands sought. From this discussion, we can only conclude that process 1 (the recombination of one exciton, exciting the other into the bottom of the

[20] R. E. Dietz, D. G. Thomas, and J. J. Hopfield, Phys. Rev. Letters 8, 391 (1962).

[21] J. L. Yarnell, J. L. Warren, R. G. Wenzel, and P. J. Dean, in *Proceedings of the International Conference on Neutron Inelastic Scattering, Copenhagen, 1968* (International Atomic Energy Agency, Vienna, 1968), p. 301.

conduction band) may have been observed, but this conclusion requires further substantiation.

VII. NATURE OF BINDING

The binding energy of the second exciton is almost as large as that of the first exciton. The A line of the single exciton lies 11 meV below the intrinsic exciton or 21 meV below the free-particle gap. Measured relative to the centers of gravity of the A-B states and the double-exciton states, the difference between the binding energies of the first and second excitons is only 1.88 meV. By contrast, for excitons bound to neutral donors, the exciton localization energy is typically only $\sim 10\%$ of the donor binding energy.[22] In silicon, the dissociation energy of the free-excitonic molecule is not known precisely, but is less than 25% of the exciton binding energy.[12]

Phillips has shown[23] that there is a cancellation effect in the binding of a particle to an isoelectronic defect. Whereas one would obtain a binding energy of the order of 1 eV for an electron bound to nitrogen in GaP from electronegativity differences alone, the lattice distorts due to an electrostrictive effect in such a manner as to reduce the binding energy practically to zero. This view is supported by an examination of the phonon side bands of the A-B transitions, which show phonon cooperation from all parts of the Brillouin zone with strong contributions from LO phonons but weak participation by momentum-conserving phonons. In contrast, for excitons bound to shallow neutral donors, much of the lattice cooperation is in the momentum-conserving phonons.

We have not been able to detect phonon sidebands of the A^*-B^* lines. Whatever phonon cooperation exists must be less than 1% of that for the A-B lines. This remarkable fact can be connected with the equally remarkable fact of the near equality of the binding energies of the first and second excitons. It appears that the additional lattice distortion accompanying the binding of the second exciton is less than 1% of the initial distortion produced in the binding of the first exciton. It also appears that this lattice response is responsible for the near equality of the binding energies.

We note that the exciton binding energies are small compared to the optical phonon energies (~ 50 meV). This means that the dynamical situation is one in which the ionic motion can follow the electronic, which is just the reverse of the usual one described by the Born-Oppenheimer approximation. Perhaps the ionic motion in the two-exciton case has almost the same amplitude as in the one-exciton case, but is phase-correlated to the electronic motion in such a way that the two electrons do not occupy the central cell at the same time. Phillips's estimates[23] suggest that each electron may spend 10% of its time in the central cell. Such a correlation might therefore reduce the binding energy of the second exciton compared to the first by about 10%, as is observed to be the case.

VIII. CONCLUSIONS

Extensive experimental and theoretical results have been presented for the A^* and B^* lines in the photoluminescence spectrum of nitrogen-doped GaP, along with their behavior in a magnetic field and their dependence on excitation intensity. This evidence demonstrates that the A^* and B^* lines result from the radiative recombination of an excitonic molecule bound at a nitrogen site. The ground states of the transitions are the A and B line states of the single bound exciton. The model proposed here eliminates the consideration of valley-orbit excited states from the single-bound-exciton problem, in contrast to earlier notions.[8,9] This is beneficial to the theory of isoelectronic binding because small energy separations between valley-orbit states implies small intervalley potential matrix elements, whereas the strong optical absorption observed for the A line implies that these matrix elements are large.[9]

The close agreement between experiment and theory for the complex magnetic behavior presented in Sec. IV is strong evidence for the correct identification of the energy states involved. In addition, the model of the bound excitonic molecule predicts two effects which have also been confirmed experimentally: (a) the square-law dependence of the A^* and B^* lines on the single-exciton lines; and (b) the possibility for Auger transitions. The investigation of (a) has also provided information about the effect of heating on the excitonic molecule, and the experimental conditions favorable for its creation.

Nonradiative Auger recombination, made possible by the presence of four particles in the excitonic molecule, has been detected by the decrease in radiative efficiency of the nitrogen luminescence as the temperature is reduced to 1.5°K. The double-exciton state is preferentially formed (and hence the Auger effect is most significant) at very low temperatures because of the large increase in the lifetime of the single-exciton transition below ~ 5°K. Thus, the most efficient nitrogen luminescence can be obtained at approximately 5°K. Thermal dissociation of the single exciton state commences between 5 and ~ 10°K. Other multiple-particle processes, where the decay of one exciton excites the second into the bottom of the conduction band or to the free exciton level, have been sought; however, the evidence for such processes is inconclusive.

The binding energy of the second exciton to the nitrogen center is almost as large as that of the first exciton. The large binding energy of the second exciton is a consequence of the nature of isoelectronic binding, being short range and substantially dynamical in origin.[23]

[22] J. R. Haynes, Phys. Rev. Letters 4, 361 (1960).
[23] J. C. Phillips, Phys. Rev. Letters 22, 285 (1969).

ACKNOWLEDGMENTS

The authors are indebted to J. C. Phillips for illuminating insights concerning the nature of the binding of the second exciton, and to J. J. Hopfield for valuable discussions. The crystals used in these experiments were grown by E. Schonherr. E. A. Sadowski assisted in much of the experimental work. The argon-ion laser was supplied by E. I. Gordon. The use of the electromagnet and Bausch and Lomb spectrograph was generously provided by C. H. Henry.

APPENDIX

In this appendix we discuss the most general linear Zeeman interactions for the states of double and single excitons bound to centers of T_d symmetry, as is appropriate for GaP:N. These general formulas are related to simple spin Hamiltonians and the appropriate g factors are derived from the directly measurable experimental quantities.

We assume the electrons are simple spin $S=\frac{1}{2}$ particles with Γ_6 symmetry.[14] For a three-valley conduction band such as that of GaP, this assumes that only the valley-orbit singlet electron state is important, that the doublet state is split off far enough in energy to produce no appreciable effect. Similarly, the holes are assumed to behave as angular momentum $J=\frac{3}{2}$ particles with Γ_8 symmetry, as is appropriate for the topmost degenerate valence band of GaP.

1. Single-Exciton States

For a state composed of one electron and one hole, the possible symmetries are $\Gamma_6\times\Gamma_8=\Gamma_3+\Gamma_4+\Gamma_5$. This corresponds to states of total angular momentum $J_t=1$ (Γ_5) and $J_t=2$ ($\Gamma_4+\Gamma_3$) with odd parity. (Of course, the group T_d does not contain the inversion, but parity is approximately conserved for the envelope functions of diffuse excitons in GaP.)

To construct the most general linear Zeeman interaction for these states, we first note that $\beta\mathbf{V}\cdot\mathbf{H}$ is the most general linear Zeeman Hamiltonian, where $\mathbf{H}$ is the applied magnetic field, β is the Bohr magneton ($\beta=eh/2mc=5.788\times10^{-6}$ eV/kG), and $\mathbf{V}$ is an operator whose components transform like Γ_4 under T_d symmetry and which change sign under time reversal. The problem reduces simply to finding matrix elements within the manifold of states Γ_3, Γ_4, and Γ_5. This can be done straightforwardly in the manner shown by Koster *et al.*[14]

The results for Γ_3, Γ_4, and Γ_5 states are shown in Table II. The entries to Table II are the matrix elements: $\langle\Gamma_i,n|\beta\mathbf{V}\cdot\mathbf{H}|\Gamma_j,m\rangle$, where $|\Gamma_i,n\rangle$ is the nth partner function of the basis comprising Γ_i symmetry. There are five independent constants in Table II: γ_1, γ_2, γ_3, δ_1, and δ_2. Time reversal requires all of these constants to be real. The diagonal entries of Table II are the zero magnetic field energy levels of the states of each symmetry.

The state of Γ_5 symmetry is the A state of the single exciton bound to nitrogen and the states $\Gamma_4+\Gamma_3$ together comprise the B state. The splitting $\epsilon_4-\epsilon_3$ is unobservably small. At low magnetic fields, γ_1 gives the splitting of the A line and γ_2 and γ_3 give the splittings of the B line. At high fields, δ_1 and δ_2 cause nonlinear shifts in the A and B lines due to mutual interactions. Thus the five constants γ_1, γ_2, γ_3, δ_1, and δ_2 are directly and independently measurable.

For a magnetic field along a $\langle001\rangle$ crystallographic direction, the eight energy levels may be obtained analytically:

$$\begin{aligned}
&E=\tfrac{1}{2}(\epsilon_3+\epsilon_4)\pm[\tfrac{1}{4}(\epsilon_3-\epsilon_4)^2+4(\gamma_3\beta H)^2]^{1/2},\\
&E=\tfrac{1}{2}(\epsilon_5+\epsilon_3)\pm[\tfrac{1}{4}(\epsilon_5-\epsilon_3)^2+4(\delta_2\beta H)^2]^{1/2},\\
&E=\tfrac{1}{2}(\epsilon_5+\epsilon_4)-\tfrac{1}{2}(\gamma_1+\gamma_2)\beta H\\
&\qquad\pm\{\tfrac{1}{4}[\epsilon_5-\epsilon_4-(\gamma_1-\gamma_2)\beta H]^2+3(\delta_1\beta H)^2\}^{1/2},\\
&E=\tfrac{1}{2}(\epsilon_5+\epsilon_4)+\tfrac{1}{2}(\gamma_1+\gamma_2)\beta H\\
&\qquad\pm\{\tfrac{1}{4}[\epsilon_5-\epsilon_4+(\gamma_1-\gamma_2)\beta H]^2+3(\delta_1\beta H)^2\}^{1/2}.
\end{aligned}\tag{A1}$$

For other directions, the matrix of Table II must be diagonalized numerically to find the energy levels.

Yafet and Thomas[2] have previously analyzed the A-B lines of GaP:N in a magnetic field. They used the

TABLE II. Magnetic interaction matrix for the states of the single exciton bound to N in GaP. There are five independent constants allowed by group theory for the interactions of these states.

		Γ_5			Γ_4			Γ_3	
		1	2	3	1	2	3	1	2
Γ_5	1	ϵ_5	$-i\gamma_1\beta H_z$	$i\gamma_1\beta H_y$	0	$-i3^{1/2}\delta_1\beta H_z$	$-i3^{1/2}\delta_1\beta H_y$	$-i3^{1/2}\delta_2\beta H_x$	$-i\delta_2\beta H_x$
	2	$i\gamma_1\beta H_z$	ϵ_5	$-i\gamma_1\beta H_x$	$-i3^{1/2}\delta_1\beta H_z$	0	$-i3^{1/2}\delta_1\beta H_x$	$i3^{1/2}\delta_2\beta H_y$	$-i\delta_2\beta H_y$
	3	$-i\gamma_1\beta H_y$	$i\gamma_1\beta H_x$	ϵ_5	$-i3^{1/2}\delta_1\beta H_y$	$-i3^{1/2}\delta_1\beta H_x$	0	0	$i2\delta_2\beta H_z$
Γ_4	1	0	$i3^{1/2}\delta_1\beta H_z$	$i3^{1/2}\delta_1\beta H_y$	ϵ_4	$i\gamma_2\beta H_z$	$-i\gamma_2\beta H_y$	$-i\gamma_3\beta H_x$	$i3^{1/2}\gamma_3\beta H_x$
	2	$i3^{1/2}\delta_1\beta H_z$	0	$i3^{1/2}\delta_1\beta H_x$	$-i\gamma_2\beta H_z$	ϵ_4	$i\gamma_2\beta H_x$	$-i\gamma_3\beta H_y$	$-i3^{1/2}\gamma_3\beta H_y$
	3	$i3^{1/2}\delta_1\beta H_y$	$i3^{1/2}\delta_1\beta H_x$	0	$i\gamma_2\beta H_y$	$-i\gamma_2\beta H_x$	ϵ_4	$i2\gamma_3\beta H_z$	0
Γ_3	1	$i3^{1/2}\delta_2\beta H_x$	$-i3^{1/2}\delta_2\beta H_y$	0	$i\gamma_3\beta H_x$	$i\gamma_3\beta H_y$	$-i2\gamma_3\beta H_z$	ϵ_3	0
	2	$i\delta_2\beta H_x$	$i\delta_2\beta H_y$	$-i2\delta_2\beta H_z$	$-i3^{1/2}\gamma_3\beta H_x$	$i3^{1/2}\gamma_3\beta H_y$	0	0	ϵ_3

spin Hamiltonian:

$$H_1=\beta[K_1\mathbf{J}\cdot\mathbf{H}+L_1(J_x^3H_x+J_y^3H_y+J_z^3H_z)+g_e\mathbf{S}\cdot\mathbf{H}], \quad \text{(A2)}$$

which is an independent sum of a hole Zeeman Hamiltonian[24] and an isotropic electron Hamiltonian. K_1 and L_1 are the isotropic and the anisotropic g factors of the hole and g_e is the g factor of the electron. This Hamiltonian is incomplete because only three parameters are included, whereas Table II shows that five parameters are needed. The accuracy of the data used by Yafet and Thomas was inadequate for the nonlinear shifts caused by δ_1 and δ_2 to be detectable. Any addition to H_1 must involve cross terms between **S** and **J** and cannot be given simple physical meanings such as are given to K_1, L_1, and g_e. We will see that such extra terms make small contributions, however.

The parameters of Table II can be related to the parameters of H_1 as follows:

$$\begin{aligned}\gamma_1&=\tfrac{1}{4}[5K_1+(41/4)L_1-g_e],\\ \gamma_2&=\tfrac{1}{4}[3K_1+(15/4)L_1+g_e],\\ \gamma_3&=\tfrac{1}{4}[3K_1+(27/4)L_1+g_e],\end{aligned} \quad \text{(A3)}$$

$$\delta_1=\tfrac{1}{4}[K_1+(13/4)L_1-g_e], \quad \delta_2=\tfrac{1}{4}[K_1+\tfrac{1}{4}L_1-g_e]. \quad \text{(A4)}$$

These equations imply an interrelationship among the five parameters obtained purely from group theory:

$$\delta_1=\tfrac{1}{2}(\gamma_1-\gamma_2), \quad \delta_2=\tfrac{1}{2}(\gamma_1+\gamma_2)-\gamma_3. \quad \text{(A5)}$$

The measured values of the five constants are shown in Table I. From the values shown there, it is seen that relations (A5) are almost satisfied, although the discrepancy is outside experimental error.

2. Double-Exciton States

For a state composed of two electrons and two holes, the possible symmetries of the electrons reduce to Γ_1 by the Pauli exclusion principle and those of the holes reduce to $\Gamma_1+\Gamma_3+\Gamma_5$. Therefore, the total symmetry of the state is $\Gamma_1+\Gamma_3+\Gamma_5$. This corresponds to states of total angular momentum $J_t=0$ (Γ_1) and $J_t=2$ ($\Gamma_3+\Gamma_5$) with even parity.

[24] J. M. Luttinger, Phys. Rev. **102**, 1030 (1956).

TABLE III. Magnetic interaction matrix for the states of the excitonic molecule bound to N in GaP. There are two independent constants allowed by group theory for the interactions of these states.

		Γ_1	Γ_5		Γ_3	
		1	1	2	3	1	2
Γ_1	1	$\bar{\epsilon}_1$	0	0	0	0	0
Γ_5	1	0	$\bar{\epsilon}_5$	$i\zeta_1\beta H_z$	$-i\zeta_1\beta H_y$	$-i3^{1/2}\zeta_2\beta H_x$	$-i\zeta_2\beta H_x$
	2	0	$-i\zeta_1\beta H_z$	$\bar{\epsilon}_5$	$i\zeta_1\beta H_x$	$i3^{1/2}\zeta_2\beta H_y$	$-i\zeta_2\beta H_y$
	3	0	$i\zeta_1\beta H_y$	$-i\zeta_1\beta H_x$	$\bar{\epsilon}_5$	0	$i2\zeta_2\beta H_z$
Γ_3	1	0	$i3^{1/2}\zeta_2\beta H_x$	$-i3^{1/2}\zeta_2\beta H_y$	0	$\bar{\epsilon}_3$	0
	2	0	$i\zeta_2\beta H_x$	$i\zeta_2\beta H_y$	$-i2\zeta_2\beta H_z$	0	$\bar{\epsilon}_3$

The most general linear Zeeman interaction among these states is found exactly as for the single exciton. It is found that a magnetic field will not mix Γ_1 with Γ_3 or Γ_5 and therefore the Γ_1 state will not shift at all for any magnetic field. The remaining interactions for Γ_3 and Γ_5 are the same as before and are displayed in Table III. There are only two independent constants in the matrix, ζ_1 and ζ_2. The zero-field energy levels are the diagonal entries in Table III.

For a magnetic field along ⟨001⟩, the six energy levels are

$$\begin{aligned}&E=\bar{\epsilon}_1, \quad E=\bar{\epsilon}_3, \quad E=\bar{\epsilon}_5\pm\zeta_1\beta H,\\ &E=\tfrac{1}{2}(\bar{\epsilon}_5+\bar{\epsilon}_3)\pm[\tfrac{1}{4}(\bar{\epsilon}_5-\bar{\epsilon}_3)^2+4(\zeta_2\beta H)^2]^{1/2}.\end{aligned} \quad \text{(A6)}$$

Because only two parameters are required in Table III, the magnetic interactions for the double exciton can be represented exactly by a spin Hamiltonian which is a simple sum of two hole Zeeman Hamiltonians[24]:

$$H_2=\beta\{K_2(\mathbf{J}_1+\mathbf{J}_2)\cdot\mathbf{H}+L_2[(J_{1x}^3+J_{2x}^3)H_x+(J_{1y}^3+J_{2y}^3)H_y+(J_{1z}^3+J_{2z}^3)H_z]\}, \quad \text{(A7)}$$

where again K_2 and L_2 are the isotropic and anisotropic g factors of the holes.

The parameters of Table III can be related to K_2 and L_2 as follows:

$$\zeta_1=(K_2+(13/4)L_2), \quad \zeta_2=(K_2+(7/4)L_2). \quad \text{(A8)}$$

Table I lists the measured values of ζ_1 and ζ_2 along with the derived values of K_2 and L_2.